Energies and lifetimes of electrons and excitons in Si_{20} modeled by many-body Green's function theory

Yi He and Taofang Zeng

Phys. Rev. B **84**, 165323 — Published 24 October 2011

DOI: 10.1103/PhysRevB.84.165323

Energies and Lifetimes of Electrons and Excitons in Si_{20} Modeled by Many-body Green's-Function Theory

Yi He and Taofang Zeng*
Department of Mechanical Engineering, Massachusetts Institute of Technology, 77 Massachusetts Avenue, Cambridge, Massachusetts 02139, USA
(Dated: October 6, 2011)

Electronic and excitonic properties in the silicon cluster Si_{20} are studied using the many-body Green's-function theory. The implementations of the self-consistencies of both the one-particle Green's function G and the reducible polarizability Π are discussed. Numerical results of the full self-consistency (FSC) and partial self-consistency (PSC) of the reducible polarizability Π are presented. It is found that the FSC implementation, where both the energies and the amplitudes of Π are updated, is numerically unstable. On the other hand, the PSC implementation, where only the energies are updated, is a stable process. The quasiparticle lifetimes in Si_{20} are calculated by the GWΓ method and can be categorized into a high-energy regime and a low-energy regime. In the high-energy regime, the scaled lifetimes of electrons and holes in Si_{20} are calculated to be 104 and 30 $\mathrm{fs\,eV^2}$ respectively, which are close to the corresponding bulk theoretical values in literatures. In the low-energy regime, the scaled quasiparticle lifetimes are found to be longer than those in the high-energy regime, which is attributed to the absence of electronic states around the Fermi level available for the transitions of hot electrons (holes). The excitonic lifetimes in Si_{20} are calculated using the dynamic Bethe-Salpeter equation (DBSE). It is found that excitonic lifetimes in a prolate structure such as Si_{20} are irrelevant to the polarization direction of the incident photons, and are solely dependent on the excitonic energies. An approximate method for calculating excitonic lifetimes based on the weighted summation of lifetimes of electrons and holes is proposed. It is demonstrated that with a much less computational cost than DBSE, the approximation can produce results closely following those of DBSE.

PACS numbers: 36.40.Cg, 36.40.Vz, 73.22.-f, 73.22.Lp

I. INTRODUCTION

Electronic and optical properties are extremely important information for the investigations and applications of semiconductor nanoclusters (SCNCs).[1] Electronic energy levels are mostly concerned in building SCNC-based devices, where energy levels need to be appropriately aligned across the heterojunctions composed of SCNCs and other materials.[2] Optical features of SCNCs represent the responses of SCNCs to the incident photons and play a key role in various optics-related applications of SCNCs.[3] Both electronic and optical characteristics of SCNCs can be obtained through spectral measurements. More specifically, electronic energy levels can be determined by the direct and inverse photoemission techniques,[4] while optical properties are usually characterized by various absorption and emission spectra.[5]

From the theoretical aspect, universal first-principles methods for the prediction of electronic and optical behaviors of materials are indispensable gears for the researches of SCNCs, especially when knowledge about the systems investigated is limited. Over the past several decades, the density functional theory (DFT) has been widely used for calculating ground-state properties of molecules and solids.[6] Within the framework of DFT, the original many-body system is replaced by a non-interacting reference system composed of independent particles. This simplification reduces the computational cost significantly, and thus makes DFT a prevailing simulation method. However, a well known issue of DFT is its tendency to underestimate the electronic bandgaps. One proper approach for calculating the properties of electrons, or more precisely, quasiparticles (QPs) including quasielectrons and quasiholes, is the GW method based on the many-body Green's-function theory.[7–9] The GW method has been proven to be accurate for the simulations of electronic structures of a vast range of materials.[8–11] The superiority of GW over DFT arises from the fact that the non-local and dynamic features of the self-energy are preserved for each QP state in the GW implementation, but not in the DFT scheme.

The interaction between SCNCs and incident photons usually involves the particle-hole excitations (or excitons) of the systems, and thus can not be correctly formulated by any method based on one-particle picture, including DFT and GW. An economic solution for the problem is the time dependent DFT (TDDFT), a method frequently used together with the adiabatic local density approximation (TDLDA).[12] TDLDA often yields right excitonic energies for finite systems. Another powerful but more cumbersome approach based on the many-body Green's-function theory is the Bethe-Salpeter equation (BSE).[12–14] BSE explicitly includes the exchange and dynamic screened Coulomb interaction between the two particles considered, and is the standard for the simulation of excitons in bulk materials where TDLDA usually fails. Furthermore, the frequency-dependent kernel of BSE enables it to capture the dynamic features of excitons, which is also beyond the scope of TDLDA.

Although electronic and excitonic energies in different SCNCs have been investigated by the GW and BSE methods,[15,16] efforts on electronic and excitonic lifetimes in SCNCs are relatively rare. In this paper, the term "lifetime" exclusively means the time scale of the electron-electron inelastic scattering in a system. Decay pathways due to non-radiative and radiative processes are not taken into account. For a hot electron (hole), the inverse of its inelastic lifetime correspond to the rate that this electron (hole) transfers its energy to the remaining electrons in the system through the inelastic scattering process. This process is the dominant decay pathway for electrons (holes) with large excitation energies. The decay rate can be evaluated as the imaginary part of the complex QP energy in the GW method,[17,18] which has incorporated such a dynamic characteristic of the system into the frequency-dependent self-energy term. The lifetime data of electrons shall be of interest for electronics based on SCNCs. Furthermore, within the theoretical framework of the many-body Green's function theory, the calculation of the electronic lifetimes in an SCNC is the starting point for the evaluation of the excitonic lifetimes in the same system, which will also be elucidated in this paper.

The inelastic lifetime of an exciton represents the rate that the exciton transfers its extra energy to the remaining electrons in the system, which is similar to that of electrons. Yet, the lifetimes of excitons are generally more important than those of electrons, since charge-conserved electron-hole excitations ($N \rightarrow N$) are more frequently encountered than charge-non-conserved quasiparticle excitations ($N \rightarrow N \pm 1$) in practical applications of SCNCs. (Here N is the initial number of the electrons in the system investigated.) A promising application of SCNCs where excitonic lifetimes are an important factor is the efficiency enhancement for single-junction photovoltaic devices based on the multiple exciton generation (MEG) process in SCNCs.[19] The mechanism of MEG is that an initial energetic exciton created by the incident photon could generate multiple excitons via the impact ionization process and thus increase the photocurrent of the photovoltaic devices. The rate of an MEG (or impact ionization) process is determined by the rate that an exciton transfers its energy partially to other electrons by generating other excitons in the same system. In other words, the rate of MEG is essentially the excitonic inelastic relaxation rate, or the inverse of the excitonic inelastic lifetime.

Investigations for MEG processes in different SCNCs have been reported in recent years,[20,21] yet there is still a controversy about the relation between the spatial confinement and the enhancement of MEG efficiency.[22,23] The difficulty is mostly due to the presence of the nonradiative relaxation that competes with the MEG process. The

phonon-assisted nonradiative relaxation process is also size dependent and manifests in experimental data, which complicates the explanation of these data. Therefore calculations for MEG rates based on first-principles theoretical simulations could be very useful to distinguish the two processes and to explain experimental data. With the capability of fully describing the two-particle interaction, BSE is a powerful tool for the simulation of MEG rates, or excitonic inelastic lifetimes. However, calculation of excitonic lifetimes within the framework of the many-body Green's-function theory requires the solution of the dynamic BSE (DBSE), which includes frequency-dependent terms and is computationally expensive. This seriously hinders the application of the method for the simulation of MEG rates in SCNCs.

In this paper, excitonic inelastic relaxation rates in a simple semiconductor cluster, Si_{20}, is investigated using DBSE. A simple method is proposed for the estimation of the excitonic lifetimes based on TDLDA and GW implementations, instead of solving the time-consuming DBSE. Results obtained by the approximation method are very close to those obtained by the DBSE. This reduces the computational cost dramatically without significant loss of accuracy for calculation of excitonic lifetimes. Numerical issues such as the self-consistencies of the one-particle Green's function G and the reducible polarizability Π are also addressed.

II. METHODOLOGY

A. Quasiparticle equation

The electronic energies of a many-body system can be obtained by solving the quasiparticle (QP) equation

$$(T + V_{\text{ext}} + V_{\text{H}})\phi_i(\mathbf{r}) + \int d\mathbf{r}' \Sigma_{\text{xc}}(\mathbf{r}, \mathbf{r}'; E_i)\phi_i(\mathbf{r}') = E_i\phi_i(\mathbf{r}), \tag{1}$$

where T is the kinetic energy operator, V_{ext} the external potential, V_{H} the Hartree potential, E_i and ϕ_i the energy and wavefunction of the ith QP, and $\Sigma_{\text{xc}}(\mathbf{r}, \mathbf{r}'; E_i)$ the exchange-correlation self-energy operator. The QP equation is solved based on the results of the density functional theory (DFT)

$$(T + V_{\text{ext}} + V_{\text{H}})\psi_i(\mathbf{r}) + V_{\text{xc}}(\mathbf{r})\psi_i(\mathbf{r}') = \epsilon_i\psi_i(\mathbf{r}), \tag{2}$$

where ϵ_i and ψ_i are the eigenvalue and eigenfunction of the ith Kohn-Sham (KS) particle respectively, and V_{xc} the exchange-correlation potential. With the assumption that the KS eigenfunctions agree well with the QP wavefunctions in most cases,[10] QP energies are usually solved with perturbative method to the first order

$$\langle\psi_i|\,\Sigma_{\text{xc}}(\mathbf{r}, \mathbf{r}'; E_i)\,|\psi_i\rangle - \langle\psi_i|\,V_{\text{xc}}(\mathbf{r})\,|\psi_i\rangle = E_i - \epsilon_i. \tag{3}$$

According to Hedin's equations[7], $\Sigma_{\text{xc}} = iGW\Gamma$ (with $\hbar = 1$), where Γ is the vertex function and G is the one-particle Green's function:

$$G(\mathbf{r}, \mathbf{r}'; E) = \sum_n \frac{\psi_n(\mathbf{r})\psi_n(\mathbf{r}')}{E - E_n + i\eta_n 0^+}, \tag{4}$$

where the coefficient η_n is $+1$ for unoccupied states and -1 for occupied states. W is the screened Coulomb interaction which can be written as $W = V + V\Pi V$. Here $V(\mathbf{r}, \mathbf{r}')$ is the Coulomb interaction, and $\Pi(\mathbf{r}, \mathbf{r}'; E)$ is the reducible polarizability which represents the linear response of the electronic density to the external perturbative potential, and can be expressed as the summation of well-defined resonant modes[24]

$$\begin{aligned}\Pi(\mathbf{r}, \mathbf{r}'; E) &= 2\sum_s \rho_s(\mathbf{r})\rho_s(\mathbf{r}') \\ &\times \left[\frac{1}{E - (\omega_s - i0^+)} - \frac{1}{E + (\omega_s - i0^+)}\right],\end{aligned} \tag{5}$$

where

$$\rho_s(\mathbf{r}) = \sum_{v,c} R_s^{v,c}\psi_v^*(\mathbf{r})\psi_c(\mathbf{r}). \tag{6}$$

The energies ω_s and amplitudes $\rho_s(\mathbf{r})$ of the reducible polarizability Π are obtained by solving the equation $\Pi = P + PV\Pi$, where $P = -iGG\Gamma$ is the irreducible polarizability. Both Σ_{xc} and Π (or W) include the vertex function

Γ. It has been shown that a consistent choice of Γ is necessary for the QP calculation.[25] In this paper, Γ is obtained by solving the equation $\Gamma = 1 + (\partial\Sigma^0/\partial G)GG\Gamma$ in the framework of the local density approximation (LDA), which is equivalent to the time-dependent LDA (TDLDA) for Π and GWΓ for $\Sigma_{\rm xc}$. More details can be found in Ref. 8 and 9.

The self-energy term $\langle\psi_i|\,\Sigma_{\rm xc}\,|\psi_i\rangle$ in Eq.(3) can be separated as an energy-independent exchange part $\langle\psi_i|\,\Sigma_{\rm x}\,|\psi_i\rangle$ and an energy-dependent correlation part $\langle\psi_i|\,\Sigma_{\rm c}\,|\psi_i\rangle$. The latter is evaluated as[26]

$$\langle\psi_i|\,\Sigma_{\rm c}\,|\psi_i\rangle = \sum_n \sum_s \frac{a_{n,s,i}}{E - E_n - \omega_s\eta_n}, \tag{7}$$

where $a_{n,s,i}$ equals $2\,\langle\psi_i\psi_n\,|(V+f_{\rm xc})|\,\rho_s\rangle\,\langle\rho_s\,|V|\,\psi_i\psi_n\rangle$ in the $GW\Gamma$ implementation.

The imaginary parts of the QP energies can be obtained by applying analytical continuation of $\Sigma_{\rm c}(\mathbf{r},\mathbf{r}';E_i)$ in the complex energy plane, and the complex QP energy $E_i - i\eta_i\gamma_i$ is calculated by solving a complex equation set numerically

$$\mathrm{Re}\,\langle\psi_i\,|\Sigma_{\rm xc}(E_i - i\eta_i\gamma_i)|\,\psi_i\rangle - \langle\psi_i\,|V_{\rm xc}|\,\psi_i\rangle = E_i - \epsilon_i, \tag{8a}$$

$$|\mathrm{Im}\,\langle\psi_i\,|\Sigma_{\rm xc}(E_i - i\eta_i\gamma_i)|\,\psi_i\rangle| = \gamma_i. \tag{8b}$$

Then the damping rate of a hot electron (hole) due to the inelastic electron-electron scattering is evaluated as[27]

$$\tau_i^{-1} = 2\,|\mathrm{Im}\,\langle\psi_i|\,\Sigma_{\rm xc}(\mathbf{r},\mathbf{r}';E_i)\,|\psi_i\rangle|\,, \tag{9}$$

where τ_i is the lifetime of the ith QP.

B. Bethe-Salpeter equation

An excitonic state of a system with N electrons essentially involves two particles, which can be investigated by the Bethe-Salpeter equation (BSE)[13,14]

$$\begin{aligned} L(1,2;1',2') &= G(1,2')G(2,1') \\ &+ \int d(33'44')G(1,3)G(3',1')\Xi(3,4';3',4)L(4,2;4',2'), \end{aligned} \tag{10}$$

where $L(1,2;1',2')$ is the two-particle correlation function, and the integral kernel $\Xi = \delta\Sigma/\delta G$. In Eq. (10) a integer label is assigned to a set of space, spin and time variables, namely $(1) = (\mathbf{x_1}, \mathrm{t}_1) = (\mathbf{r_1}, \sigma_1, \mathbf{t_1})$. The Fourier transformation of the terms related to the particle-hole excitations of L can be written as[14,28]

$$\begin{aligned} L^{\rm ph}(\mathbf{x}_1,\mathbf{x}_2;\mathbf{x}_{1'},\mathbf{x}_{2'}|t_1,t_{1'};\omega) &= \int_{-\infty}^{+\infty} dt_2 e^{-i\omega t_2} L^{\rm ph}(\mathbf{x}_1 t_1,\mathbf{x}_2 t_2;\mathbf{x}_{1'}t_{1'},\mathbf{x}_{2'}t_2^+) \\ &= -ie^{-i\omega(t^1-|\tau_1|/2)}\sum_r \frac{\chi_r(\mathbf{x}_1,\mathbf{x}_{1'};\tau_1)\tilde{\chi}_r(\mathbf{x}_2,\mathbf{x}_{2'};-\delta)}{\omega-\Omega_r+i\eta}e^{-i\Omega_r|\tau_1|/2} \\ &\quad +ie^{-i\omega(t^1+|\tau_1|/2)}\sum_r \frac{\chi_r(\mathbf{x}_2,\mathbf{x}_{2'};-\delta)\tilde{\chi}_r(\mathbf{x}_1,\mathbf{x}_{1'};\tau_1)}{\omega+\Omega_r-i\eta}e^{-i\Omega_r|\tau_1|/2}, \end{aligned} \tag{11}$$

where the time variables have been reorganized as

$$t^1 = \frac{t_1+t_{1'}}{2}, t^2 = \frac{t_2+t_{2'}}{2}, \tau_1 = t_1 - t_{1'}, \tau_2 = t_2 - t_{2'}. \tag{12}$$

t_2^+ means $t_2+\delta$ with $\delta\to 0^+$. Ω_r and $\chi_r(\mathbf{x}_i,\mathbf{x}_j;t_i-t_j)$ are the energy and particle-hole amplitude of the rth excitation. With the quasiparticle approximation, χ_r can be expressed as

$$\chi_r(\mathbf{x},\mathbf{x}';\tau) \approx e^{i\Omega_r|\tau|/2}\sum_{v',c'} A^r_{v'c'}\psi_{c'}(\mathbf{x})\psi^*_{v'}(\mathbf{x}')\left[e^{-i(E_{c'}-i\gamma_{c'})\tau}\theta(\tau) - e^{-i(E_{v'}+i\gamma_{v'})\tau}\theta(-\tau)\right], \tag{13}$$

where $\mathbf{A}^r$ is the eigenvector corresponding to χ_r. Note that the finite QP lifetimes have been taken into account in Eq. (13). This approach has been applied to the study of the dynamics of core-excitons in semiconductors by Strinati.[29] The integral kernel Ξ in Eq. (10) can be approximated as

$$\begin{aligned} \Xi(3,4';3',4) \approx &-i\delta(3,3')\delta(4^+,3')V(3,4) \\ &+i\delta(3,4)\delta(3',4')W(3^+,3'). \end{aligned} \tag{14}$$

By substituting Eqs. (11), (13) and (14) into Eq. (10) and projecting both sides onto $\psi_c(\mathbf{x}_1)\psi_v^*(\mathbf{x}_{1'})$ and $\chi_r(\mathbf{x}_2, \mathbf{x}_{2'}; -\delta)$, the BSE Eq. (10) can be converted to a complex eigenvalue problem

$$\begin{aligned}&\left[(E_c - i\gamma_c) - (E_v + i\gamma_v)\right] A^r_{vc} + \\ &\sum_{v'c'} A^r_{v'c'}(K^x_{vcv'c'} + K^d_{vcv'c'}) = (\Omega_r - i\Gamma_r)A^r_{vc},\end{aligned} \tag{15}$$

where Γ_r is the imaginary energy of the rth exciton. In this paper, only singlet excitations are considered, and thus the exchange term $K^x_{vcv'c'} = 2\langle\psi_v\psi_c|V|\psi_{v'}\psi_{c'}\rangle$. The direct interaction term $K^d_{vcv'c'}$ can be calculated as

$$\begin{aligned}K^d_{vcv'c'} =& -\langle\psi_v\psi_{v'}|V|\psi_c\psi_{c'}\rangle \\ &-\sum_s\left[\frac{1}{\Omega_r - i\Gamma_r - \omega_s - (E_{c'} - E_v)} + \frac{1}{\Omega_r - i\Gamma_r - \omega_s - (E_c - E_{v'})}\right] \\ &\times\left[\langle\psi_v\psi_{v'}|V|\rho_s\rangle\langle\rho_s|(V + f_{\rm xc})|\psi_c\psi_{c'}\rangle + \langle\psi_v\psi_{v'}|(V + f_{\rm xc})|\rho_s\rangle\langle\rho_s|V|\psi_c\psi_{c'}\rangle\right],\end{aligned} \tag{16}$$

where the screened interaction

$$W = V + \left[(V + f_{\rm xc})\Pi V + V\Pi(V + f_{\rm xc})\right]/2, \tag{17}$$

has been substituted into Eq. (16). Note that W is written in a symmetric form, since the local exchange-correlation effect $f_{\rm xc}$ has to be included to make Eq. (15) consistent with the calculation of $\Sigma_{\rm c}$ and Π in Sec. II A. In Eq. (15), only resonant part is taken into account, while the anti-resonant part is neglected. This is the Tamm-Dancoff approximation (TDA), whose effect on excitonic energies is found to be negligible.[13] Usually ω_s and ρ_s come from the reducible polarizability Π obtained by TDLDA (Eq. (5)).

Solution of the complex eigenvalue $\Omega_r - i\Gamma_r$ through Eq. (15) simultaneously determines the excitation energy Ω_r and the lifetime $T_r = (2\Gamma_r)^{-1}$ of the rth exciton. Actually Eq. (15) explicitly includes four terms related to the decay of the exciton, which are illustrated by the Feynman diagrams in Fig. 1. However, it is unfeasible to solve the DBSE Eq. (15) directly, since the matrix on the left hand side is explicitly dependent on the eigenvalues Ω_r to be solved. Thus Eq. (15) is usually simplified by taking the two approximations

$$\Gamma_r = \gamma_c = \gamma_v = 0, \tag{18a}$$

$$\Omega_r \approx E_{c'} - E_v \approx E_c - E_{v'}. \tag{18b}$$

which lead to an energy-independent matrix, namely the static BSE (SBSE). The reducible polarizability $\tilde{\Pi}$ obtained from SBSE can be written in the same way as that from TDLDA

$$\begin{aligned}\tilde{\Pi}(\mathbf{r}, \mathbf{r}'; E) =& 2\sum_r \tilde{\rho}_r(\mathbf{r})\tilde{\rho}^*_r(\mathbf{r}') \\ &\times\left[\frac{1}{E - (\Omega_r - i0^+)} - \frac{1}{E + (\Omega_r - i0^+)}\right],\end{aligned} \tag{19}$$

where $\tilde{\rho}_r(\mathbf{r}) = \chi_r(\mathbf{r}, \mathbf{r}, 0)$ and the tilde distinguishes the results of BSE from those of TDLDA. Note that in most cases $\tilde{\Pi}$ in Eq. (19) is different from Π in Eq. (5). The issue for the self-consistency of the reducible polarizability Π will be discussed in Sec. III A.

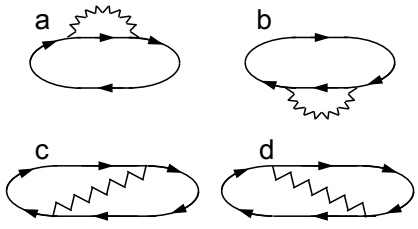

FIG. 1. Feynman diagrams of terms in Eq. (15) related to the decay of particle-hole excitations. Arrowed lines are Green's functions. Wiggled lines are screened interactions. Diagrams a and b correspond to the diagonal elements in Eq. (15). Diagrams c and d denote the screened particle-hole interaction in Eq. (16).

C. Numerical Details

The ground state LDA calculation of Si_{20} is performed using the SIESTA code.[30] Core electrons $[1s^2 2s^2 2p^6]$ of Si are replaced by the nonlocal norm-conserving pseudopotential based on the Troullier-Martins scheme.[31] A triple-ζ polarization (TZP) basis set of numerical atomic orbitals is used for the valance electrons of Si. Two stable geometric configurations of Si_{20} have been reported in literatures, one with the C_{3v} symmetry (Fig. 2a)[32,33] and the other with the C_{2h} symmetry (Fig. 2b)[34]. The former has been shown to be more stable by DFT with generalized gradient approximation (GGA) functionals, DFT with hybrid functionals and coupled-cluster CCSD(T) method. In this work, both configurations are calculated via DFT with LDA, and we find that the energy of the C_{3v} isomer is about 0.2 eV lower than the C_{2h} one. Thus all numerical work and discussion in the remaining part of the paper will focus on the structure as shown in Fig. 2a.

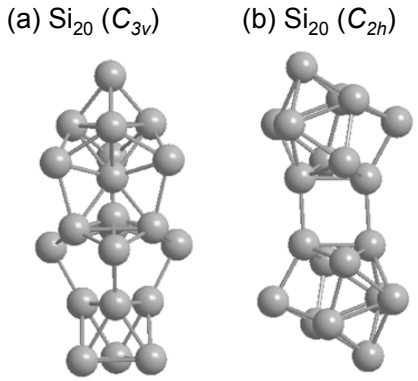

FIG. 2. Optimized structures of two isomers of Si_{20}. The labels in brackets correspond to the point group symmetries of the clusters.

All integrals are evaluated on a uniform grid in real space with grid spacing of 0.5 a.u., which has been tested to give QP energies with an accuracy of 0.1 eV. The exchange integrals $\int d\mathbf{r} \int d\mathbf{r}' \psi_i(\mathbf{r})\psi_j(\mathbf{r})V(\mathbf{r},\mathbf{r}')\psi_k(\mathbf{r}')\psi_l(\mathbf{r}')$ are evaluated by first solving Poisson equations with the multigrid method.[35] The convergence of the QP calculation usually requires a large number of unoccupied states for the evaluation of the polarizability. Thus a Coulomb-hole screened-exchange (COHSEX) remainder scheme has been applied to accelerate the convergence of the correlation part $\langle\psi_i|\,\Sigma_c\,|\psi_i\rangle$.[26]

III. RESULTS AND DISCUSSIONS

A. Self-consistency of G and Π

In the QP calculations, a ready starting point is the approximation for G

$$G(\mathbf{r},\mathbf{r}';E) \approx G_0(\mathbf{r},\mathbf{r}';E) = \sum_n \frac{\psi_n(\mathbf{r})\psi_n(\mathbf{r}')}{E-\epsilon_n+i\eta_n 0^+}. \tag{20}$$

From G_0, one can evaluate Σ_{xc} as $\Sigma_{xc} = G[V + (V + f_{xc})\Pi V]$, and thus solve the Eq. (1) for QP energies E_n. However, it not clear whether one should recalculate every quantity involved (G, Π, Σ_{xc}) until the convergence of all quantities, or the self-consistency. For calculation of QP inelastic decay rates in finite systems, we have demonstrated that it is necessary to implement the self-consistency of G,[36] which will be restated briefly here.

The inelastic decay rate of the ith QP can be written as a summation S_i

$$S_i = 2\left|\sum_n \sum_s \frac{a_{n,s,i}\gamma_i}{(E_i - E_n - \omega_s\eta_n)^2 + \gamma_i^2}\right|. \tag{21}$$

Replacing G with G_0 changes the positions of the poles from $E_n + \omega_s\eta_n$ to $\epsilon_n + \omega_s\eta_n$, which may cause considerable error to S_i, since S_i is mostly determined by the arrangement of the poles in the vicinity of E_i. The effect is illustrated schematically in Fig. 3, where unoccupied (occupied) energy levels ϵ_n obtained by DFT are shifted up (down) to yield the QP energy levels E_n. Yet the poles $\epsilon_n + \omega_s\eta_n$ are not moved together, leading to misplaced poles around a given energy level E_i.

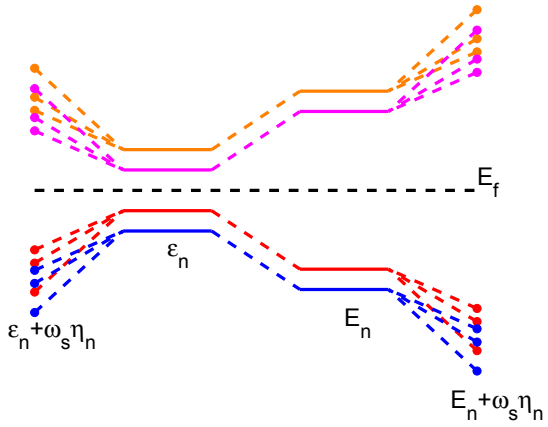

FIG. 3. Schematic plot for the relation among LDA energies ϵ_n and hence derived poles $\epsilon_n + \omega_s\eta_n$, QP energies E_n and hence derived poles $E_n + \omega_s\eta_n$. Each color defines a set including an energy level and poles accompanying the energy level. To maintain correct orders, E_n should be used together with $E_n + \omega_s\eta_n$. A mixture between E_n and $\epsilon_n + \omega_s\eta_n$ changes the pole arrangement in the vicinity of a QP energy level, which may introduce notable errors for the QP lifetimes.

In our former paper,[36] we only implement the iteration $(G \to \Sigma_{\rm xc} \to G)$, with the assumption that $\Pi \equiv \Pi_{\rm TDLDA}$. In this paper, we further extend our investigation about the self-consistency of Π. The reason for the implementation of the self-consistency of Π is similar to that of G. Since the inelastic decay rate of rth exciton can be written as a summation $\tilde{S}_r$, which also has a set of poles. Replacing Ω_s by ω_s thus changes the positions of the poles, and causes error to $\tilde{S}_r$.

Note that G is connected to all one-particle properties, namely QP energies E_n in $\Sigma_{\rm xc}$ and QP energy differences $(E_c - E_v)$ in the BSE kernel K. While Π is connected to all two-particle properties, namely excitonic energies Ω_s in both $\Sigma_{\rm xc}$ and K. If two different data sets (G', Π') and (G'', Π'') are used for $\Sigma_{\rm xc}$ and K respectively, potential confusion and inconsistency will occur. This implies that the same G and Π shall be used in the calculation of $\Sigma_{\rm xc}$ and K, which brings about a self-consistent issue at higher level, namely a cycle $(G, \Pi) \to (\Sigma_{\rm xc}, K) \to (G, \Pi)$. The relation of the three self-consistent cycles are illustrated in Fig. 4, where bold lines indicate iterative steps. The left part is the G cycle, where the self-consistent G is solved with Π as an argument. The right part is the Π cycle, where the self-consistent Π is solved with G as an argument. The central part is the $G\Pi$ cycle, which indicates the convergence of all of the four quantities. This cycle is implemented in the way $G(\Pi) \to \Pi(G) \to G(\Pi)$, until the simultaneous convergence of both G and Π.

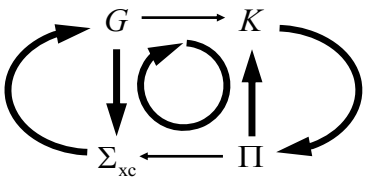

FIG. 4. Schematic plot for the three self-consistent cycles. Bold lines indicate iterative steps. The left part $G \to \Sigma_{\rm xc} \to G$ is the G cycle. The right part $\Pi \to K \to \Pi$ is the Π cycle. The central part is the $G\Pi$ cycle which is implemented in the way $G(\Pi) \to \Pi(G) \to G(\Pi)$, until the simultaneous convergence of both G and Π.

The criteria for the convergence of G and Π are required for the numerical implementation. According to Eq. (4), G is characterized by the QP wavefunctions $\psi_n(\mathbf{r})$ and the energies E_n. Usually the QP wavefuctions can be assumed to be identical to the LDA wavefunctions, then the convergence of G is simplified to the convergence of E_n. Similarly, the polarizability Π is characterized by the amplitudes $\rho_s(\mathbf{r})$ and the energies Ω_s. However, the convergence of Π has not been well studied. In this paper we test two possible implementations: the full self-consistency (FSC) and the partial self-consistency (PSC). In the FSC strategy, both the convergence of $\rho_s(\mathbf{r})$ and Ω_s are pursued, while in the PSC, only Ω_s are updated in each iteration, with $\rho_s(\mathbf{r})$ fixed to the TDLDA amplitudes. The latter essentially takes the BSE kernel as a first order correction to the TDLDA kernel, which is an analogy to the assumption made in the QP calculations that QP wavefuctions and LDA wavefunctions are identical. Note that only the static BSE is used in both the FSC and PSC tests, since the dynamic BSE is much more time-consuming, and only has minor effects on the excitonic energies Ω_s.

The QP energies and optical spectra obtained by the FSC implementation are shown in the top and bottom diagrams of Fig. 5. The arrows between the two diagrams signify the order of each numerical step. It is found that the QP energies shift toward the Fermi level as the iteration progresses. Also, the optical spectra change dramatically between two consecutive iterative steps. Both diagrams indicate that the FSC is numerically unstable. On the other hand, results obtained by the PSC implementation are more stable, as shown in Fig. 6 with the same style as Fig. 5. In PSC both the QP energies and optical spectra change only slightly after each iterative step, and converge after 2-3 cycles. Therefore our discussion about properties of QPs and excitons in Sec. III B and III C will focus on the results calculated by the PSC strategy.

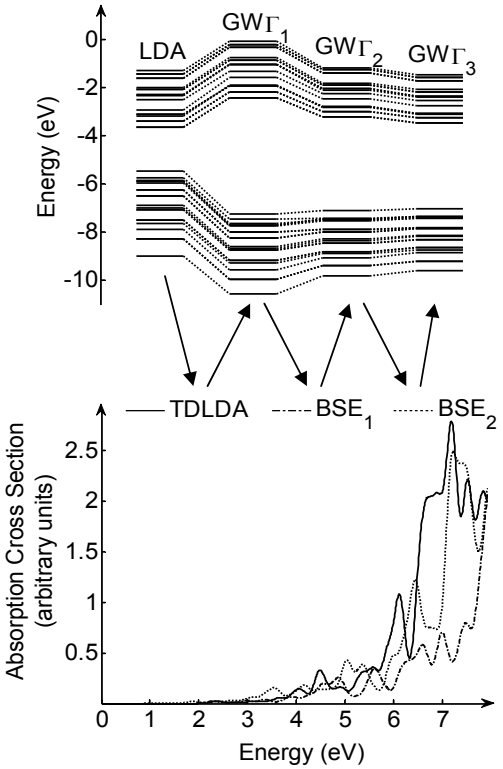

FIG. 5. QP energies (top) and optical spectra (bottom) obtained by the FSC implementation. The arrows between the two diagrams signify the order of each numerical step, namely LDA-TDLDA-GWΓ-BSE-GWΓ-BSE-GWΓ.

The significant difference between the PSC and FSC approaches arises solely from whether the amplitudes $\rho_s(\mathbf{r})$ are fixed to TDLDA ones or not during each iterative step. Thus we analyze the $\rho_s(\mathbf{r})$ calculated by TDLDA and those obtained by SBSE to reveal the crucial role of the issue. In Fig. 7, the weights of largest transition components of the first three excitations calculated by TDLDA and SBSE are illustrated. According to Fig. 7, both the TDLDA kernel and the SBSE kernel tend to mix the independent-particle transitions. The tendency of the mixture is much stronger in the case of SBSE, as the weight of the largest transition component of each SBSE exciton is smaller than that of the corresponding TDLDA exciton. This effect has been reported for BSE calculations of various systems.[16,37] It is speculated that the numerical instability of the FSC implementation could be attributed to the differences of the transition weights obtained by TDLDA and BSE. In fact, each amplitude $\rho_s(\mathbf{r})$ corresponds to a vector $\mathbf{R}_s$, and the reducible polarizability Π is a set composed of such vectors. This means that any quantity depending on Π is essentially a function of these vectors. Since TDLDA and BSE are based on different frameworks (independent-particle vs. quasiparticle), their vector sets also differ from each other, as can be seen in Fig. 7. Change from the TDLDA vector set to the BSE vector set seems to be too large for the iteration to remain in the numerical stability domain.

B. QP energies and lifetimes in Si_{20}

The QP energies in Si_{20} calculated by the GWΓ method have been illustrated in Fig. 8. The vertical ionization potential obtained by LDA is 5.46 eV, while it is adjusted to 7.22 eV by the GWΓ method. This number is close to the experimental data 7.46-7.53 eV.[38]

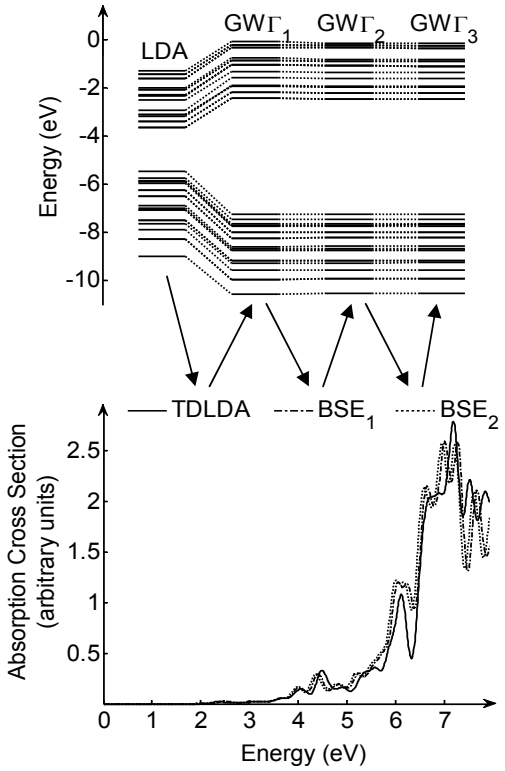

FIG. 6. QP energies (top) and optical spectra (bottom) obtained by the PSC implementation. Plotted in the same style as Fig. 5.

Inelastic lifetimes τ_i of hot electrons and holes in Si_{20} are plotted versus the excitation energy $|E_i - E_F|$ in Fig. 8a. In a high-density free electron gas (FEG), lifetimes of hot electrons with low excitation energies follow an inverse quadratic law according to Quinn and Ferell[39]

$$\tau_i^{\mathrm{QF}} = 263 r_s^{-5/2} (E_i - E_F)^{-2}\,\mathrm{eV}^2\,\mathrm{fs}. \tag{22}$$

Eq. (22) implies a constant scaled lifetime $\tau_i(E_i - E_F)^2$ for all hot electrons in FEG. Therefore we plot the scaled lifetimes of both electrons and holes as a reference in Fig. 8b, although silicon is a semiconductor with non-uniform electron gas. We find that the scaled hole lifetimes with low excitation energies ($|E_i - E_F| < 6.2\,eV$) are longer than those with high excitation energies ($|E_i - E_F| \geq 6.2\,eV$), so do the scaled electron lifetimes (with one exception). This feature is strikingly similar to that of the metallic cluster Mg_{40} simulated by the same method,[36] where a low energy regime (R_{LE}) and a high energy regime (R_{HE}) have also been observed. The similarity between the QP lifetimes in bulk silicon and those in jellium model has also been demonstrated by Fleszar and Hanke.[40] Same as the case of Mg_{40}, here the longer QP scaled lifetimes in the R_{LE} than those in the R_{HE} is also attributed to the lack of electronic states around the Fermi level available for the transitions of hot electrons (holes).[36]

In the regime R_{HE}, the scaled lifetimes of hot electrons fluctuate in the range of 90 to 150 $\mathrm{fs\,eV^2}$, with an average of 104 $\mathrm{fs\,eV^2}$. The scaled lifetimes of hot holes in this regime approach 30 $\mathrm{fs\,eV^2}$ smoothly with increasing $|E_i - E_F|$. QP lifetimes in bulk silicon have been calculated in Ref. 40 and 41. According to Fig. 2 in Ref. 41, the scaled lifetimes of electrons and holes are estimated to be 120 and 40 $\mathrm{fs\,eV^2}$ respectively, which are close to the results obtained in this paper. This implies even in a cluster as small as Si_{20}, the scaled QP lifetimes in the R_{HE} have already approached the corresponding bulk values. The notably shorter lifetimes of hot holes than those of hot electrons with the same $|E_i - E_F|$, can be attributed to the smaller angular momentums of holes, or more overlap among different hole states, which leads to more possible transitions than electrons. This is an analogy to the bulk, where one can attribute shorter hole lifetimes in simple *s-p* systems (no localized *d*-states) to the smaller momentums of holes.[42]

It is interesting to compare the semiconductor cluster Si_{20} simulated in this paper with the metallic cluster Mg_{40} studied before in Ref. 36, since both clusters have the same number of valence electrons. In Mg_{40}, the scaled lifetimes of hot electrons fluctuate in the range of 21 to 24 $\mathrm{fs\,eV^2}$, while those of hot holes are around 12 $\mathrm{fs\,eV^2}$ and decrease slightly with increasing excitation energy $|E_i - E_F|$. The results indicate that at the same excitation energy $|E_i - E_F|$, the scaled QP lifetimes in Mg_{40} are shorter than those in Si_{20}. One reason for this phenomenon is the

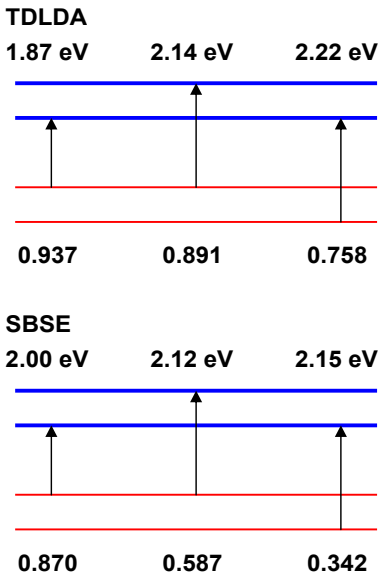

FIG. 7. Weights of the largest transition components of the first three excitons obtained by TDLDA and SBSE. Excitonic energies are also given at the top. Bold lines stand for degenerate E states, slim lines stand for non-degenerate A_1 states.

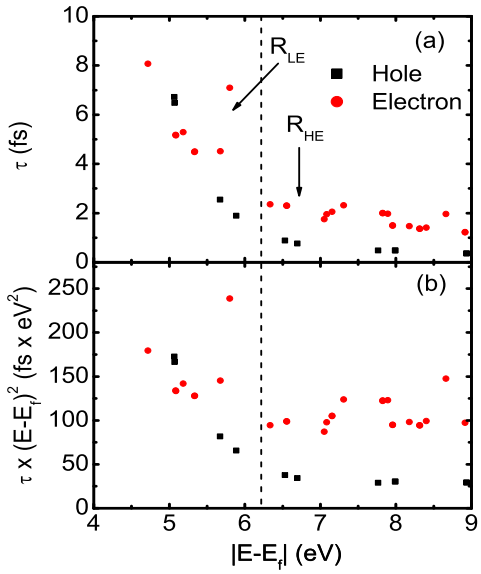

FIG. 8. (a) QP lifetimes and (b) scaled QP lifetimes in Si_{20} obtained by the self-consistent GWΓ approach. The vertical dashed line separates both plots into a low-energy regime and a high-energy regime.

larger HOMO-LUMO gap in Si_{20} than that in Mg_{40}, which leads to fewer energy states, or decaying channels, for QPs in Si_{20}. However, even if one takes this issue into account by redefining the excitation energy as $E_i - E_{\mathrm{LUMO}}$ and $E_{\mathrm{HOMO}} - E_i$ for electrons and holes, the QP lifetimes in Si_{20} are still longer, which can be explained as higher electron density in Si_{20} and thus stronger screening effects.

C. Excitonic energies and lifetimes in Si_{20}

The final excitonic energies and lifetimes are calculated via Eq. (15), in the partially self-consistent way as has been implemented in Sec. III A. Thus only complex eigenvalues are updated iteratively by the frequency-dependent dynamic BSE matrix, with eigenvectors fixed to the TDLDA amplitudes. To accelerate and stabilize the self-consistency

procedure, the initial guess for the imaginary part of the excitation energy Γ_r for a given exciton is estimated as

$$\Gamma_r = \sum_{v,c} |R^r_{vc}|^2 (\gamma_c + \gamma_v). \tag{23}$$

The absorption spectra calculated by dynamic BSE and static BSE, both with partial self-consistency, are plotted in Fig. 9. Since the cluster Si_{20} is a prolate cluster with C_{3v} symmetry as shown in Fig. 2, it exhibits A_1 transitions (electric dipole perturbation along the z-axis) and E transitions (electric dipole perturbation within the xy-plane), which are illustrated in Fig. 9a and 9b respectively. As shown in Fig. 9, the absorptive features of the A_1 transitions emerge in the lower energy regime than the E transitions, which is attributed to the larger dimension and thus less electronic confinement along the z-axis than those along the x and y-axes. On the other hand, the DBSE and SBSE absorption spectra for each irreducible representation are similar, indicating the negligible influence of the dynamic screening effect on the excitonic energies. This observation is demonstrated more clearly in Fig. 10 by plotting the energy differences between the DBSE and SBSE contribution arising from the second term in Eq. (16), where the two methods are different from each other. As shown in Fig. 10, the energy differences vary from -0.2 to 0.1 eV, with the average of -0.07 eV, which is negligible. These results demonstrate the feasibility of SBSE, which has been widely used for simulations of materials.

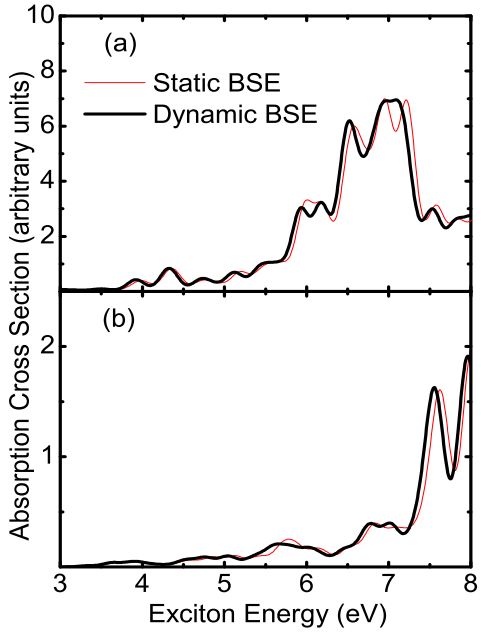

FIG. 9. Absorption spectra of (a) A_1 transitions and (b) E transitions calculated by the dynamic and static BSE, both with partial self-consistency. Absorption lines are broadened by Gaussian lineshapes with a spectral width of 0.1 eV.

The excitonic inelastic decay rates (MEG rates) Γ_r of A_1 and E transitions vs. excitonic energies Ω_r are plotted in log-log style in Fig. 11. Although the two transition modes differ in terms of the positions of major absorption peaks, their decay-rate patterns almost coincide with each other. The results indicate that the excitonic lifetimes are geometry-insensitive, and are solely determined by the excitation energy. We fit the data point with a simple rational function (Padé function P_1^2),

$$y = 2x + a + \frac{b}{x + c}, \tag{24}$$

where x and y represent $\ln(\Omega/\text{eV})$ and $\ln(\Gamma/\text{eV})$ respectively. The fitting coefficients a, b and c are -4.49, -0.98 and -1.19. Here the coefficient of the linear term is fixed to be 2, since it is easy to prove that the quadratic relation between the excitonic decay rate and the excitonic energy will be approached at high-energy limit (large x) for both single-particle excitations and collective excitations, provided that the quadratic relation between the QP decay rate and the QP energy is approached at the high-energy regime as in this case. According to Eq. (24), excitons with energies 5.0, 6.0 and 7.0 eV shall have lifetimes 12, 4.2, 2.2 fs respectively. The results provide a general picture about the MEG rate: the process occurs on a time scale of several to several tens of femtoseconds in the silicon cluster investigated.

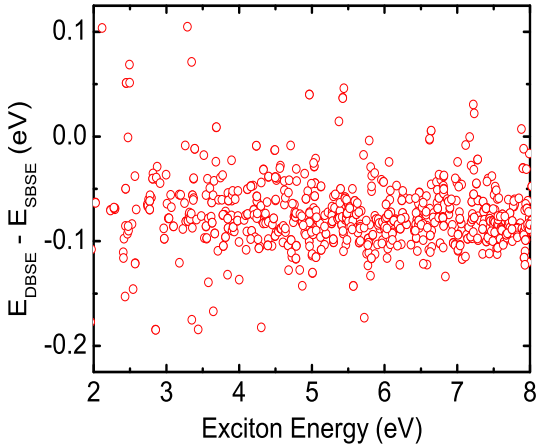

FIG. 10. Energy differences between the DBSE and SBSE contribution arising from the second term in Eq. (16), with the negative sign included.

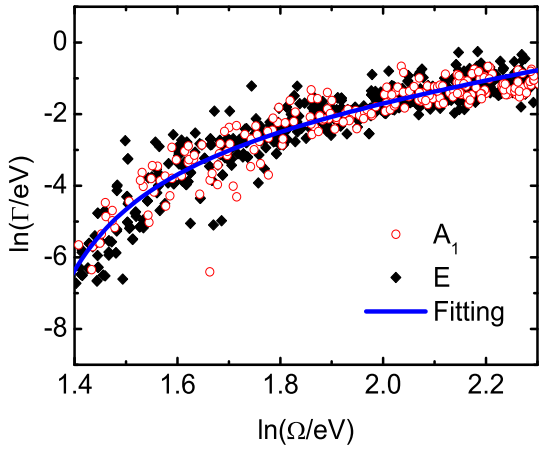

FIG. 11. Log-Log plot of excitonic inelastic decay rates Γ_r of A_1 and E transitions vs. excitonic energies Ω_r. The solid line is the rational curve-fitting of the data points.

The most interesting issue is how the excitonic decay rates estimated based on Eq. (23) differ from those obtained by solving the dynamic BSE(DBSE). If results calculated by the two approaches are close, then Eq. (23) can replace DBSE in the calculation of excitonic lifetimes, which can reduce the computational time dramatically. Actually the difference of the two approaches can be understood in terms of Feynman diagrams: Eq. (23) only takes into account the first two diagrams in Fig. 1, while the dynamic BSE applied in this paper includes all the four diagrams in Fig. 1.

The ratios of the excitonic inelastic decay rates calculated with DBSE over those obtained with Eq. (23) are plotted as a function of the excitonic energies in Fig. 12, where the ratios are again geometry-insensitive according to the patterns of A_1 and E transitions. Furthermore, one can find that for excitons in the high-energy regime ($\Omega_r > 4.5\,\mathrm{eV}$), their ratios can be fitted by a constant (0.966) as shown by the solid line. The number is close to unity, indicating Eq. (23) is a very good approximation of the DBSE results for excitonic decay rates in the high-energy regime. The fitted constant is slightly smaller than unity, which means inclusion of the dynamic screening effect (the last two diagrams in Fig. 1) reduces excitonic decay rates for most excitons. This is similar to the conclusion in Ref. 29, where core-excitation width Γ is predicted to be smaller than core-hole width γ by inclusion of the dynamic screening effects when solving BSE. Note that the MEG effect can only be observed for incident photons with energies larger than twice the optical bandgap. For Si_{20} the optical bandgaps obtained by different methods (TDLDA, SBSE and DBSE) are around 2.0 eV, which means that the excitonic MEG energy threshold should be about 4.0 eV. Therefore the lower values in Fig. 12 located around 4.0 eV indicate that the approximation method tends to overestimate especially near the MEG energy threshold, with the maximum factor of about 1.9 in our case.

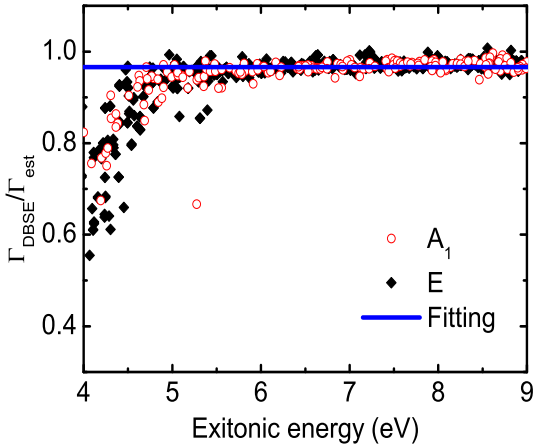

FIG. 12. Ratios of the excitonic inelastic decay rates calculated with DBSE over those estimated by Eq. (23) for A_1 and E transitions. The solid line is the constant curve-fitting of the data points in the high-energy regime.

IV. CONCLUSION

In this paper, we simulate the electronic and excitonic properties in the silicon cluster Si_{20}. The implementations of the self-consistencies of the one-particle Green's function G and the reducible polarizability Π within the framework of the many-body Green's-function theory are discussed. The full self-consistency of Π, where both the amplitudes $\rho_s(\mathbf{r})$ and the energies Ω_s are allowed to relax, is numerically unstable. On the other hand, the partial self-consistency of Π is stable where only the energies Ω_s are allowed to relax. The scaled lifetimes of electrons and holes in the high-energy regime are predicted to be 104 and 30 $\mathrm{fs\,eV^2}$, which are close to the corresponding bulk values. The scaled QP lifetimes in the low-energy regime are longer than those in the high-energy regime due to the lack of electronic states around the Fermi level available for the transitions of hot electrons (holes). The excitonic inelastic decay rates in Si_{20} are calculated by dynamic Bethe-Salpeter equation (DBSE), and estimated by the weighted summation method based on QP lifetimes. Results from the two methods are close to each other. With much less computational cost than DBSE, the approximate method thus provides a fast way for the calculation of excitonic inelastic lifetimes in SCNCs. We also found that excitonic lifetimes are solely dependent on the excitonic energies, and are insensitive to the geometry of the structures.

ACKNOWLEDGMENTS

This project is sponsored by the National Science Foundation (Grant CTS-0500402/CBET-0830098).

* tzeng2@mit.edu

[1] A. Yoffe, Adv. Phys. **50**, 1 (2001).
[2] P. V. Kamat, J. Phys. Chem. C **112**, 18737 (2008).
[3] W. C. W. Chan and S. Nie, Science **281**, 2016 (1998).
[4] V. L. Colvin, A. P. Alivisatos, and J. G. Tobin, Phys. Rev. Lett. **66**, 2786 (1991).
[5] D. J. Norris and M. G. Bawendi, Phys. Rev. B **53**, 16338 (1996).
[6] R. M. Martin, *Electronic Structure, Basic Theory and Practical Methods*, (Cambridge University Press, Cambridge, 2004).
[7] L. Hedin, Phys. Rev. **139**, A796 (1965).
[8] W. G. Aulbur, L. Jönsson, and J. W. Wilkins, in *Solid State Physics*, edited by F. Seitz, D. Turnbull, and H. Ehrenreich, vol. 54, p. 1, (Academic, New York, 2000).
[9] F. Aryasetiawan and O. Gunnarsson, Rep. Prog. Phys. **61**, 237 (1998).
[10] M. S. Hybertsen and S. G. Louie, Phys. Rev. B **34**, 5390 (1986).
[11] R. W. Godby, M. Schlüter, and L. J. Sham, Phys. Rev. B **37**, 10159 (1988).
[12] G. Onida, L. Reining, and A. Rubio, Rev. Mod. Phys. **74**, 601 (2002).
[13] M. Rohlfing and S. G. Louie, Phys. Rev. B **62**, 4927 (2000).
[14] G. Strinati, Riv. Nuovo Cimento **11**, 1 (1988).
[15] L. X. Benedict, A. Puzder, A. J. Williamson, J. C. Grossman, G. Galli, J. E. Klepeis, J.-Y. Raty, and O. Pankratov, Phys. Rev. B **68**, 085310 (2003).
[16] M. Lopez del Puerto, M. L. Tiago, and J. R. Chelikowsky, Phys. Rev. B **77**, 045404 (2008).
[17] P. M. Echenique, J. M. Pitarke, E. V. Chulkov, and A. Rubio, Chem. Phys. **251**, 1 (2000).
[18] E. V. Chulkov, A. G. Borisov, J. P. Gauyacq, D. Sánchez-Portal, V. M. Silkin, V. P. Zhukov and, P. M. Echenique, Chem. Rev. **106**, 415 (2006).
[19] A. J. Nozik, Physica E **14**, 115 (2002).
[20] R. D. Schaller and V. I. Klimov, Phys. Rev. Lett. **92**, 186601 (2004).
[21] M. C. Beard, K. P. Knutsen, P. Yu, J. M. Luther, Q. Song, W. K. Metzger, R. J. Ellingson, and A. J. Nozik, Nano Lett. **7**, 2506 (2007).
[22] G. Nair, L. Y. Chang, S. M. Geyer, and M. G. Bawendi, Nano Lett. **11**, 2145 (2011).
[23] M. T. Trinh, A. J. Houtepen, J. M. Schins, T. Hanrath, J. Piris, W. Knulst, A. P. L. M. Goossens, and L. D. A. Siebbeles, Nano Lett. **8**, 1713 (2008).
[24] M. E. Casida, in *Recent Advances in Density-Functional Methods, Part I*, edited by D. P. Chong (World Scientific, Singapore, 1995), p. 155.
[25] R. Del Sole, L. Reining, and R. W. Godby, Phys. Rev. B **49**, 8024 (1994).
[26] M. L. Tiago and J. R. Chelikowsky, Phys. Rev. B **73**, 205334 (2006).
[27] G. D. Mahan, *Many-Particle Physics*, 3rd ed. (Kluwer/Plenum, New York, 2000).
[28] C. Csanak, H. S. Taylor, and R. Yaris, Adv. At. Mol. Phys. **7**, 287 (1971).
[29] G. Strinati, Phys. Rev. B **29**, 5718 (1984).
[30] J. M. Soler, E. Artacho, J. D. Gale, A. García, J. Junquera, P. Ordejón, and D. Sánchez-Portal, J. Phys. Condens. Matter **14**, 2745 (2002).
[31] N. Troullier and J. L. Martins, Phys. Rev. B **43**, 1993 (1991).
[32] I. Rata, A. A. Shvartsburg, M. Horoi, T. Frauenheim, K. W. Michael Siu, and K. A. Jackson, Phys. Rev. Lett. **85**, 546 (2000).
[33] S. Yoo and X. C. Zeng, J. Chem. Phys. **123**, 164303 (2005).
[34] L. Mitas, J. C. Grossman, I. Stich and J. Tobik, Phys. Rev. Lett. **84**, 1479 (2000).
[35] U. Trottenberg, C. W. Oosterlee, and A. Schüller, *Multigrid*, (Academic, San Diego, 2001).
[36] Y. He and T. F. Zeng, Phys. Rev. B **84**, 035456 (2011).
[37] M. Rohlfing and S. G. Louie, Phys. Rev. Lett. **80**, 3320 (1998).
[38] K. Fuke, K. Tsukamoto, F. Misaizu, and M. Sane, J. Chem. Phys. **99** 7807 (1993).
[39] J. J. Quinn and R. A. Ferrell, Phys. Rev. **112**, 812 (1958).
[40] A. Fleszar and W. Hanke, Phys. Rev. B **56**, 10228 (1997).
[41] B. Arnaud, S. Lebégue, and M. Alouani, Phys. Rev. B **71**, 035308 (2005).
[42] I. Campillo, A. Rubio, J. M. Pitarke, A. Goldmann, and P. M. Echenique, Phys. Rev. Lett. **85**, 3241 (2000).